



**University of  
Zurich**<sup>UZH</sup>

**Zurich Open Repository and  
Archive**

University of Zurich  
University Library  
Strickhofstrasse 39  
CH-8057 Zurich  
[www.zora.uzh.ch](http://www.zora.uzh.ch)

---

Year: 2011

---

## Dalitz plot analysis of $D_s^+ \rightarrow K^+ K^- \pi^+$

BABAR Collaboration ; del Amo Sanchez, P ; Snoek, H L

**Abstract:** We perform a Dalitz plot analysis of about 100 000  $D_s^+$  decays to  $K^+ K^- \pi^+$  and measure the complex amplitudes of the intermediate resonances which contribute to this decay mode. We also measure the relative branching fractions of  $D_s^+ \rightarrow K^+ K^- \pi^+$  and  $D_s^+ \rightarrow K^+ K^- K^0$ . For this analysis we use a 384 fb<sup>-1</sup> data sample, recorded by the BABAR detector at the PEP-II asymmetric-energy e<sup>+</sup>e<sup>-</sup> collider running at center-of-mass energies near 10.58 GeV.

DOI: <https://doi.org/10.1103/PhysRevD.83.052001>

Other titles: Dalitz plot analysis of  $D_s^+ \rightarrow K^+ K^- \pi^+$

Posted at the Zurich Open Repository and Archive, University of Zurich

ZORA URL: <https://doi.org/10.5167/uzh-58693>

Journal Article

Accepted Version

Originally published at:

BABAR Collaboration; del Amo Sanchez, P; Snoek, H L (2011). Dalitz plot analysis of  $D_s^+ \rightarrow K^+ K^- \pi^+$ . Physical Review D, 83(5):052001.

DOI: <https://doi.org/10.1103/PhysRevD.83.052001>

# Dalitz Plot Analysis of $D_s^+ \rightarrow K^+ K^- \pi^+$

R. E. Mitchell,<sup>1</sup> M. R. Shepherd,<sup>1</sup> D. Besson,<sup>2</sup> T. K. Pedlar,<sup>3</sup> J. Xavier,<sup>3</sup>  
D. Cronin-Hennessy,<sup>4</sup> K. Y. Gao,<sup>4</sup> J. Hietala,<sup>4</sup> Y. Kubota,<sup>4</sup> T. Klein,<sup>4</sup> R. Poling,<sup>4</sup>  
A. W. Scott,<sup>4</sup> P. Zweber,<sup>4</sup> S. Dobbs,<sup>5</sup> Z. Metreveli,<sup>5</sup> K. K. Seth,<sup>5</sup> B. J. Y. Tan,<sup>5</sup>  
A. Tomaradze,<sup>5</sup> J. Libby,<sup>6</sup> L. Martin,<sup>6</sup> A. Powell,<sup>6</sup> C. Thomas,<sup>6</sup> G. Wilkinson,<sup>6</sup>  
H. Mendez,<sup>7</sup> J. Y. Ge,<sup>8</sup> D. H. Miller,<sup>8</sup> I. P. J. Shipsey,<sup>8</sup> B. Xin,<sup>8</sup> G. S. Adams,<sup>9</sup> D. Hu,<sup>9</sup>  
B. Moziak,<sup>9</sup> J. Napolitano,<sup>9</sup> K. M. Ecklund,<sup>10</sup> Q. He,<sup>11</sup> J. Insler,<sup>11</sup> H. Muramatsu,<sup>11</sup>  
C. S. Park,<sup>11</sup> E. H. Thorndike,<sup>11</sup> F. Yang,<sup>11</sup> M. Artuso,<sup>12</sup> S. Blusk,<sup>12</sup> S. Khalil,<sup>12</sup>  
R. Mountain,<sup>12</sup> K. Randrianarivony,<sup>12</sup> N. Sultana,<sup>12</sup> T. Skwarnicki,<sup>12</sup> S. Stone,<sup>12</sup>  
J. C. Wang,<sup>12</sup> L. M. Zhang,<sup>12</sup> G. Bonvicini,<sup>13</sup> D. Cinabro,<sup>13</sup> M. Dubrovin,<sup>13</sup> A. Lincoln,<sup>13</sup>  
M. J. Smith,<sup>13</sup> P. Naik,<sup>14</sup> J. Rademacker,<sup>14</sup> D. M. Asner,<sup>15</sup> K. W. Edwards,<sup>15</sup> J. Reed,<sup>15</sup>  
A. N. Robichaud,<sup>15</sup> G. Tatishvili,<sup>15</sup> E. J. White,<sup>15</sup> R. A. Briere,<sup>16</sup> H. Vogel,<sup>16</sup>  
P. U. E. Onyisi,<sup>17</sup> J. L. Rosner,<sup>17</sup> J. P. Alexander,<sup>18</sup> D. G. Cassel,<sup>18</sup> J. E. Duboscq,<sup>18,\*</sup>  
R. Ehrlich,<sup>18</sup> L. Fields,<sup>18</sup> L. Gibbons,<sup>18</sup> R. Gray,<sup>18</sup> S. W. Gray,<sup>18</sup> D. L. Hartill,<sup>18</sup>  
B. K. Heltsley,<sup>18</sup> D. Hertz,<sup>18</sup> J. M. Hunt,<sup>18</sup> J. Kandaswamy,<sup>18</sup> D. L. Kreinick,<sup>18</sup>  
V. E. Kuznetsov,<sup>18</sup> J. Ledoux,<sup>18</sup> H. Mahlke-Krüger,<sup>18</sup> J. R. Patterson,<sup>18</sup> D. Peterson,<sup>18</sup>  
D. Riley,<sup>18</sup> A. Ryd,<sup>18</sup> A. J. Sadoff,<sup>18</sup> X. Shi,<sup>18</sup> S. Stroiney,<sup>18</sup> W. M. Sun,<sup>18</sup> T. Wilksen,<sup>18</sup>  
J. Yelton,<sup>19</sup> P. Rubin,<sup>20</sup> N. Lowrey,<sup>21</sup> S. Mehrabyan,<sup>21</sup> M. Selen,<sup>21</sup> and J. Wiss<sup>21</sup>

(CLEO Collaboration)

<sup>1</sup>*Indiana University, Bloomington, Indiana 47405, USA*

<sup>2</sup>*University of Kansas, Lawrence, Kansas 66045, USA*

<sup>3</sup>*Luther College, Decorah, Iowa 52101, USA*

<sup>4</sup>*University of Minnesota, Minneapolis, Minnesota 55455, USA*

<sup>5</sup>*Northwestern University, Evanston, Illinois 60208, USA*

<sup>6</sup>*University of Oxford, Oxford OX1 3RH, UK*

<sup>7</sup>*University of Puerto Rico, Mayaguez, Puerto Rico 00681*

<sup>8</sup>*Purdue University, West Lafayette, Indiana 47907, USA*

<sup>9</sup>*Rensselaer Polytechnic Institute, Troy, New York 12180, USA*

<sup>10</sup>*Rice University, Houston, TX 77005, USA*

<sup>11</sup>*University of Rochester, Rochester, New York 14627, USA*

<sup>12</sup>*Syracuse University, Syracuse, New York 13244, USA*

<sup>13</sup>*Wayne State University, Detroit, Michigan 48202, USA*

<sup>14</sup>*University of Bristol, Bristol BS8 1TL, UK*

<sup>15</sup>*Carleton University, Ottawa, Ontario, Canada K1S 5B6*

<sup>16</sup>*Carnegie Mellon University, Pittsburgh, Pennsylvania 15213, USA*

<sup>17</sup>*Enrico Fermi Institute, University of Chicago, Chicago, Illinois 60637, USA*

<sup>18</sup>*Cornell University, Ithaca, New York 14853, USA*

<sup>19</sup>*University of Florida, Gainesville, Florida 32611, USA*

<sup>20</sup>*George Mason University, Fairfax, Virginia 22030, USA*

<sup>21</sup>*University of Illinois, Urbana-Champaign, Illinois 61801, USA*

(Dated: 6 March 2009)

## Abstract

We perform a Dalitz plot analysis of the decay  $D_s^+ \rightarrow K^+ K^- \pi^+$  with the CLEO-c data set of  $586 \text{ pb}^{-1}$  of  $e^+e^-$  collisions accumulated at  $\sqrt{s} = 4.17 \text{ GeV}$ . This corresponds to about 0.57 million  $D_s^\pm D_s^{*\mp}$  pairs from which we select 14400 candidates with a background of roughly 15%. In contrast to previous measurements we find good agreement with our data only by including an additional  $f_0(1370)\pi^+$  contribution. We measure the magnitude, phase, and fit fraction of  $K^*(892)^0 K^+$ ,  $\phi(1020)\pi^+$ ,  $K_0^*(1430)K^+$ ,  $f_0(980)\pi^+$ ,  $f_0(1710)\pi^+$ , and  $f_0(1370)\pi^+$  contributions and limit the possible contributions of other  $KK$  and  $K\pi$  resonances that could appear in this decay.

---

\*Deceased

## I. INTRODUCTION

The decay  $D_s^+ \rightarrow K^+ K^- \pi^+$  is among the largest known branching fractions for the  $D_s$  meson. For some time the mode  $D_s^+ \rightarrow \phi(1020)\pi^+$  was used as the normalizing mode for  $D_s$  decay branching fractions, typically done by choosing events with the  $K^+ K^-$  invariant mass near the narrow  $\phi(1020)$  peak. Observation of a large contribution from  $D_s^+ \rightarrow f_0(980)\pi^+$  [1] makes the selection of  $D_s^+ \rightarrow \phi(1020)\pi^+$  dependent on the range of  $K^+ K^-$  invariant mass chosen; the observed yield of non- $\phi$  contributions can be larger than 10% [2]. This is an unacceptably large uncertainty for a normalizing mode and we proposed [2] that the branching fraction for  $D_s^+ \rightarrow K^+ K^- \pi^+$  in the neighborhood of the  $\phi$  peak, without any attempt to identify the  $\phi\pi^+$  component as such, could be used for  $D_s$  normalization. Relating the  $D_s^+ \rightarrow K^+ K^- \pi^+$  branching fraction in [2] to the rates for such phase space-restricted subsets requires an understanding of the resonance contributions to the final state. The only published Dalitz plot analysis [3] has been done by E687 [1] using 701 signal events. The FOCUS Collaboration has studied this decay in a Dalitz plot analysis in an unpublished thesis [4] and a conference presentation [5].

Here we describe a Dalitz plot analysis of  $D_s^+ \rightarrow K^+ K^- \pi^+$  using the CLEO-c data set which yields a sample of over 12,000 signal candidates. Charge conjugation is implied throughout except where explicitly mentioned. The next section describes our experimental techniques, the third section gives our Dalitz plot analysis formalism, the fourth describes our fits to the data, and there is a brief conclusion.

## II. EXPERIMENTAL TECHNIQUE

CLEO-c is a general purpose detector which includes a tracking system for measuring momenta and specific ionization of charged particles, a Ring Imaging Cherenkov detector to aid particle identification, and a CsI calorimeter for detection of electromagnetic showers. These components are immersed in a magnetic field of 1 T, provided by a superconducting solenoid, and surrounded by a muon detector. The CLEO-c detector is described in detail elsewhere [6].

We reconstruct the  $D_s^+ \rightarrow K^+ K^- \pi^+$  decay using three tracks measured in the tracking system. Charged tracks satisfy standard goodness of fit quality requirements [7]. Pion and kaon candidates are required to have specific ionization,  $dE/dx$ , in the main drift chamber within four standard deviations of the expected value at the measured momentum.

We use two kinematic variables to select  $D_s^+ \rightarrow K^+ K^- \pi^+$  decays, the candidate invariant mass

$$m_{\text{inv}} \equiv m(K^+ K^- \pi^+) \quad \text{or} \quad \Delta m_{\text{inv}} = m_{\text{inv}} - m_{D_s}, \quad (1)$$

and the beam constrained mass

$$m_{\text{BC}} = \sqrt{E_{\text{beam}}^2 - p_D^2} \quad \text{or} \quad \Delta m_{\text{BC}} = m_{\text{BC}} - m_{\text{BC}}(D_s), \quad (2)$$

where  $m_{D_s}=1968.2$  MeV/ $c^2$  [8] is the  $D_s$  mass,  $E_{\text{beam}}$  is the beam energy,  $p_D$  is the momentum of reconstructed  $D_s^+$  candidate, and  $m_{\text{BC}}(D_s) = 2040.25$  MeV/ $c^2$  is the expected  $m_{\text{BC}}$  value of the  $D_s$  meson in the process  $e^+e^- \rightarrow D_s^* D_s$  at  $\sqrt{s} = 4170$  MeV. We require  $|\Delta m_{\text{inv}}| < 2\sigma(m_{\text{inv}})$ ,  $|\Delta m_{\text{BC}}| < 2\sigma(m_{\text{BC}})$ , where the resolutions  $\sigma(m_{\text{inv}}) = 4.8$  MeV/ $c^2$  ( $4.79 \pm 0.05$  MeV/ $c^2$  in single Gaussian fit), and  $\sigma(m_{\text{BC}}) = 2$  MeV/ $c^2$  ( $1.89 \pm 0.02$  MeV/ $c^2$ )

represent the widths of the signal peak in the two dimensional distribution. When there are multiple  $D_s$ -meson candidates in a single event we select the one with smallest  $\Delta m_{BC}$  value.

We use a kinematic fit to all 3-track combinations which enforces a common vertex and  $D_s^+$  mass constraint. The kinematic fit-corrected 4-momenta of all 3 particles are used to calculate invariant masses for further Dalitz plot analysis. The resolution on the resonance invariant mass is almost always better than  $5 \text{ MeV}/c^2$ .

After all requirements, we select 14400 candidate events for the Dalitz plot analysis. The fraction of background, 15.1%, in this sample is estimated from the fits to the  $m_{\text{inv}}$  spectrum shown in Figure 1. In most fits to the Dalitz plot we constrain the value of the

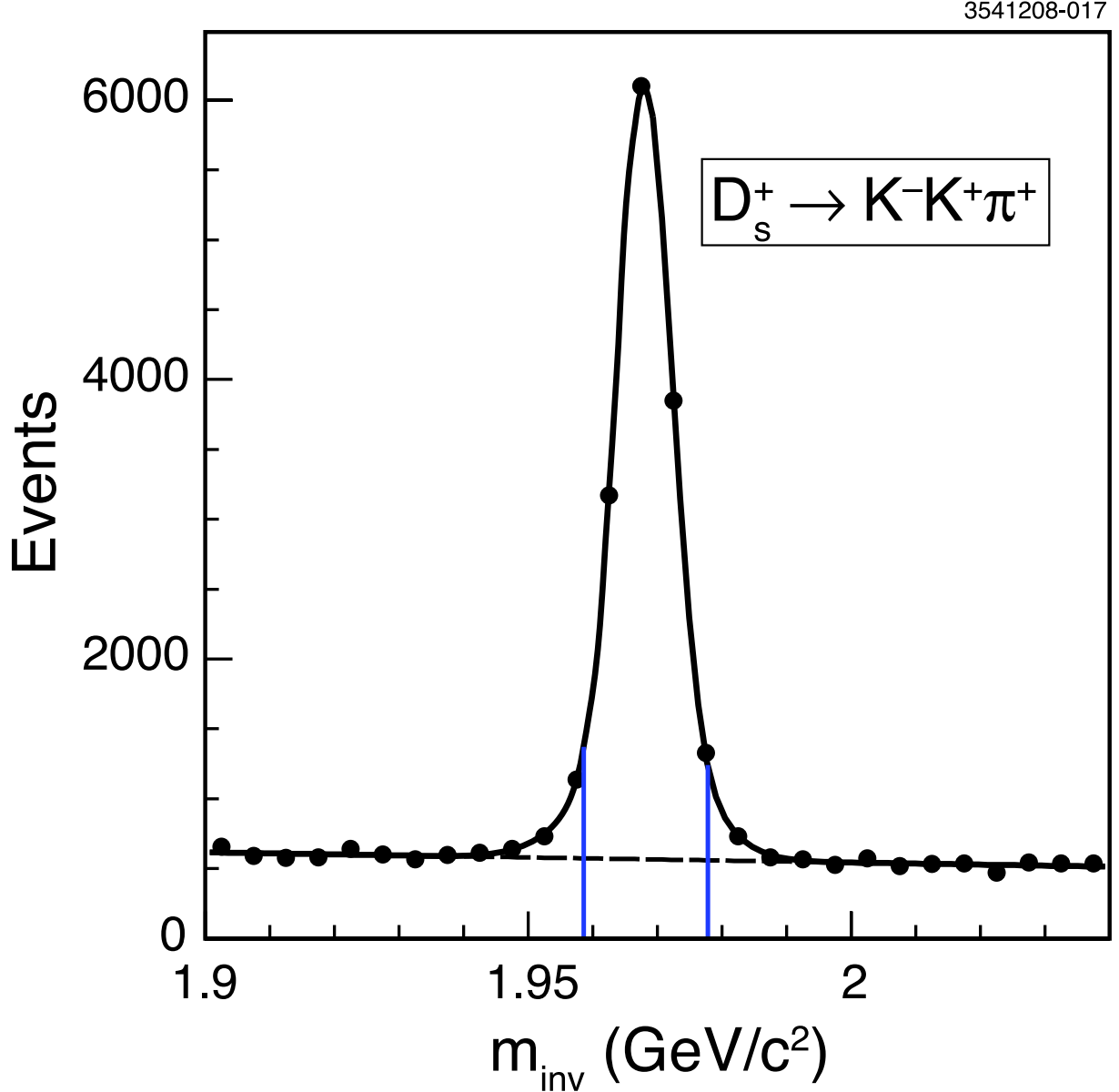


FIG. 1: The  $m_{\text{inv}}$  distribution. The vertical (online blue) lines show the  $\pm 2\sigma$  signal region.

signal fraction,  $f_{\text{sig}} = 84.90 \pm 0.15\%$ . In cross checks we use a set of sub-samples, splitting the data by time of observation and by sign of  $D_s$ -meson charge,  $D_s^+$  and  $D_s^-$ . We also consider

samples with tight ( $1 \times 1$  standard deviations in  $m_{\text{BC}}$  and  $m_{\text{inv}}$ ) and loose ( $3 \times 3$  three standard deviations) selection versus the standard selection, as well as samples of  $D_s$  mesons produced in  $D_s^* \rightarrow D_s \gamma$  decays, selected with a displaced signal box using  $m_{\text{BC}}$  low band ( $|m_{\text{BC}} - 2025 \text{ MeV}/c^2| < 4\sigma(m_{\text{BC}})$ ) and  $m_{\text{BC}}$  high band ( $|m_{\text{BC}} - 2060 \text{ MeV}/c^2| < 4\sigma(m_{\text{BC}})$ ).

To determine the efficiency we use a signal Monte-Carlo (MC) [9] simulation where one of the charged  $D_s$  mesons decays in the  $KK\pi$  mode uniformly in the phase space, while the other  $D_s$  meson decays in all known modes with relevant branching fractions. In total we generated  $10^6$   $D_s^+$  and  $D_s^-$  signal decays. These underlying events are input to the CLEO-c detector simulation and processed with the CLEO-c reconstruction package. The MC-generated events are required to pass the same selection requirements as data selected in the signal box. We only select the signal-side  $D_s$  mesons which decay uniformly in the phase space, separating them by charge.

We analyze events on the Dalitz plot by choosing  $x = m^2(K^+K^-)$  and  $y = m^2(K^-\pi^+)$  as the independent  $(x, y)$  variables. The third variable  $z = m^2(K^+\pi^+)$  is dependent on  $x$  and  $y$  through energy and momentum conservation. We do not expect any resonant sub-structure in the  $K^+\pi^+$  invariant mass; with these Dalitz plot variables any structure in  $z$  is due to reflections of structures in  $x$  and  $y$ . Figure 2 shows the Dalitz plot. Besides the clear  $\phi(1020)$  and  $K^*(892)$  signal, no other narrow features are clearly observed. The variation of the population density along the resonance band clearly indicates that these resonances are spin one as the amplitude for a spin-one resonance should have a node in the middle of its band. There is a significant population density in the node region of the  $\phi(1020)$  resonance, indicating that there is likely to be an additional contribution.

To parametrize the efficiency,  $\varepsilon(x, y)$ , we use a third-order polynomial function with respect to the arbitrary point  $(x_c, y_c) = (2, 1) \text{ (GeV}/c^2)^2$  on the Dalitz plot times threshold functions in each of the Dalitz variables to account for the loss of efficiency at the edges of the Dalitz plot, such that

$$\varepsilon(x, y) = \varepsilon_{\text{poly}}(x, y)T(x)T(y)T(z(x, y)). \quad (3)$$

With  $\hat{x} = x - x_c$  and  $\hat{y} = y - y_c$ , the efficiency is the product of the polynomial function,

$$\varepsilon_{\text{poly}}(x, y) = 1 + E_x \hat{x} + E_y \hat{y} + E_{x^2} \hat{x}^2 + E_{y^2} \hat{y}^2 + E_{x^3} \hat{x}^3 + E_{y^3} \hat{y}^3 + E_{xy} \hat{x} \hat{y} + E_{x^2 y} \hat{x}^2 \hat{y} + E_{xy^2} \hat{x} \hat{y}^2, \quad (4)$$

For each Dalitz plot variable,  $v$  ( $\equiv x, y$  or  $z$ ) the threshold function is sine-like with

$$T(v) = \begin{cases} [E_{c,v} + (1 - E_{c,v})] \times \sin(E_{\text{th},v} \times |v - v_{\text{max}}|), & \text{at } 0 < E_{\text{th},v} \times |v - v_{\text{max}}| < \pi/2, \\ 1, & \text{at } E_{\text{th},v} \times |v - v_{\text{max}}| \geq \pi/2, \end{cases} \quad (5)$$

All polynomial coefficients,  $E_x$ ,  $E_y$ ,  $E_{x^2}$ ,  $E_{y^2}$ ,  $E_{x^3}$ ,  $E_{y^3}$ ,  $E_{xy}$ ,  $E_{x^2 y}$ ,  $E_{xy^2}$ ,  $E_{c,v}$ , and  $E_{\text{th},v}$  are fit parameters. Each variable  $v$  has two thresholds,  $v_{\text{min}}$  and  $v_{\text{max}}$ . We expect low efficiency in the regions  $v \approx v_{\text{max}}$  only, where one of three particles is produced with zero momentum in the  $D_s$  meson rest frame and thus has a small momentum in the laboratory frame.

The simulated signal sample is used to determine the efficiency. Table I shows the results of the fit to the entire signal MC sample of  $D_s^+ \rightarrow K^+ K^- \pi^+$  events selected on the Dalitz plot. The polynomial function with threshold factors describes the efficiency shape very well for our sample. We also fit separately the signal MC sub-samples for  $D_s^+ \rightarrow K^+ K^- \pi^+$  and  $D_s^- \rightarrow K^- K^+ \pi^-$  decays, for simulations of early and late datasets, and for tight and loose signal boxes. In cross-checks with sub-samples we fix the threshold parameters to their values from the central fit in order to remove correlations with other polynomial parameters.

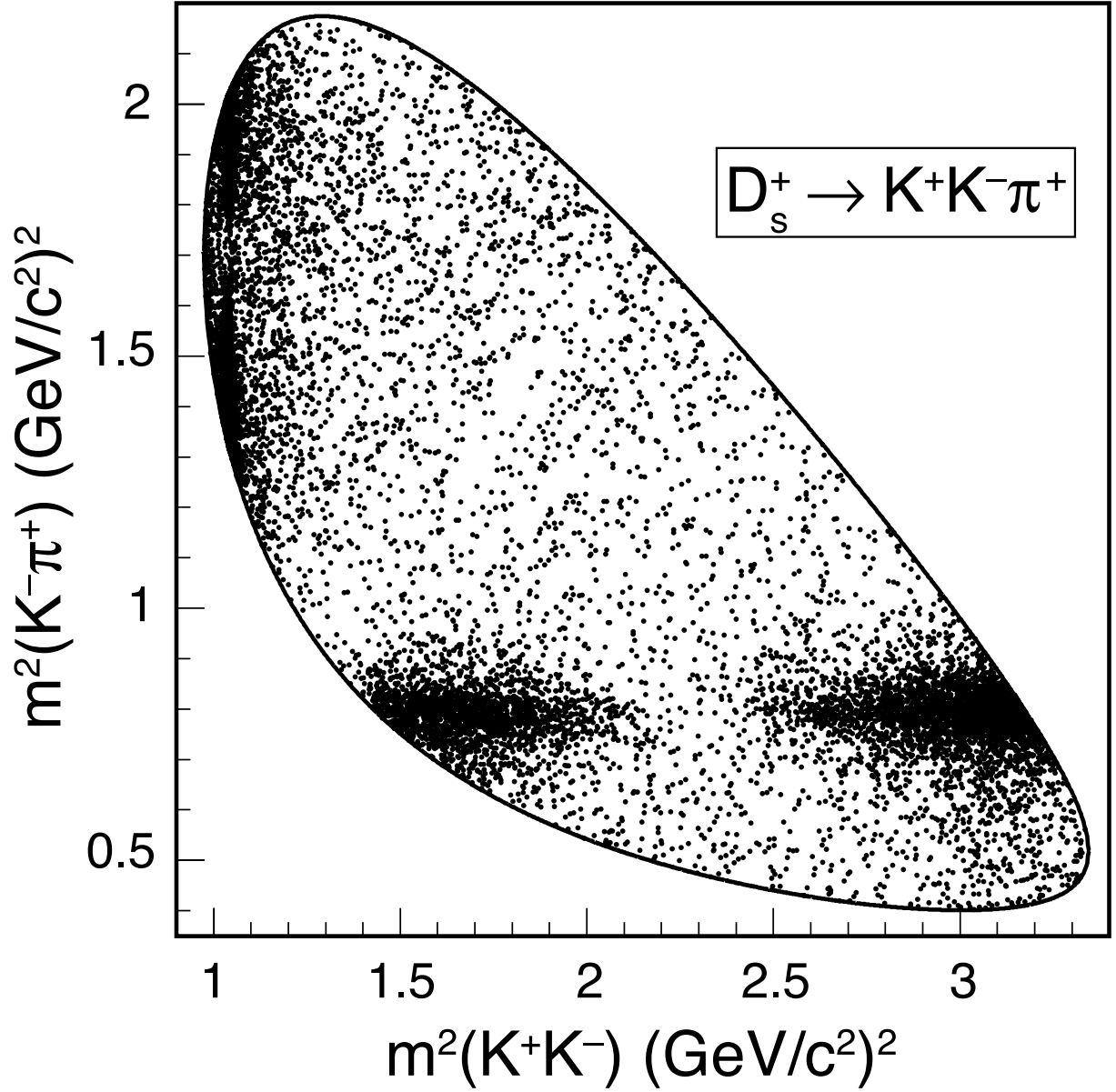


FIG. 2: The Dalitz plot for the data.

We find that the variation of the efficiency polynomial parameters is small compared to their statistical uncertainties. In fits to data we use this efficiency shape with fixed parameters, and constrained variation is allowed as a systematic check.

The shape for the background on the Dalitz plot is estimated using data events from a  $m_{\text{BC}}$  sideband region,  $|m_{\text{BC}} - 1900 \text{ MeV}/c^2| < 5\sigma(m_{\text{BC}})$ . We only consider events from the low mass  $m_{\text{BC}}$  sideband as the high mass sideband is contaminated by signal events due to initial state radiation. To parametrize the background shape on the Dalitz plot we employ a function similar to that used for the efficiency, shown in Eq. 4. We add incoherently to the polynomial two peaking contributions to represent  $K^*(892)$  and  $\phi(1020)$  contributions described with Breit-Wigner functions with floating normalization coefficients,  $B_{K^*}$  and  $B_\phi$ , respectively. Figure 3 and Table II show results of the fit to the background polynomial

TABLE I: Fit parameters for describing the efficiency across the Dalitz plot.

Parameter	Value
$E_x$	$0.023 \pm 0.012$
$E_y$	$0.037 \pm 0.014$
$E_{x2}$	$-0.307 \pm 0.014$
$E_{xy}$	$-0.526 \pm 0.034$
$E_{y2}$	$-0.201 \pm 0.034$
$E_{x3}$	$0.262 \pm 0.026$
$E_{x2y}$	$0.953 \pm 0.078$
$E_{xy2}$	$0.887 \pm 0.098$
$E_{y3}$	$0.004 \pm 0.051$
$E_{th,x}$	$3.23 \pm 0.18$
$E_{th,y}$	$2.53 \pm 0.13$
$E_{th,z}$	$2.61 \pm 0.13$
$E_{c,x}$	$0.166 \pm 0.042$
$E_{c,y}$	$0.320 \pm 0.034$
$E_{c,z}$	$0.338 \pm 0.034$

TABLE II: Fit parameters for the background sample. Values in parentheses show an uncertainty or variation of the last significant digits.

Parameter	Value
$B_x$	$-0.23 \pm 0.11$
$B_y$	$0.06 \pm 0.13$
$B_{x2}$	$-0.29 \pm 0.12$
$B_{xy}$	$-0.99 \pm 0.29$
$B_{y2}$	$-0.47 \pm 0.32$
$B_{x3}$	$0.77 \pm 0.23$
$B_{x2y}$	$1.98 \pm 0.67$
$B_{xy2}$	$2.24 \pm 0.84$
$B_{y3}$	$0.56 \pm 0.47$
$B_\phi$	$0.000161(23)$
$B_{K^*}$	$0.00144(28)$

function for our sample. We also consider the variation of the background shape parameters for sub-samples, split for  $D_s^+$  and  $D_s^-$ , for earlier and later datasets, and for tight and loose cuts on background selection box. The variation of the shape parameters is small compared to their statistical uncertainties. Furthermore, in fits to data we use the background shape with fixed parameters, and constrained variation is allowed as a systematic cross check. We also allow the size of the narrow resonance contributions to the background to float freely as a systematic variation.



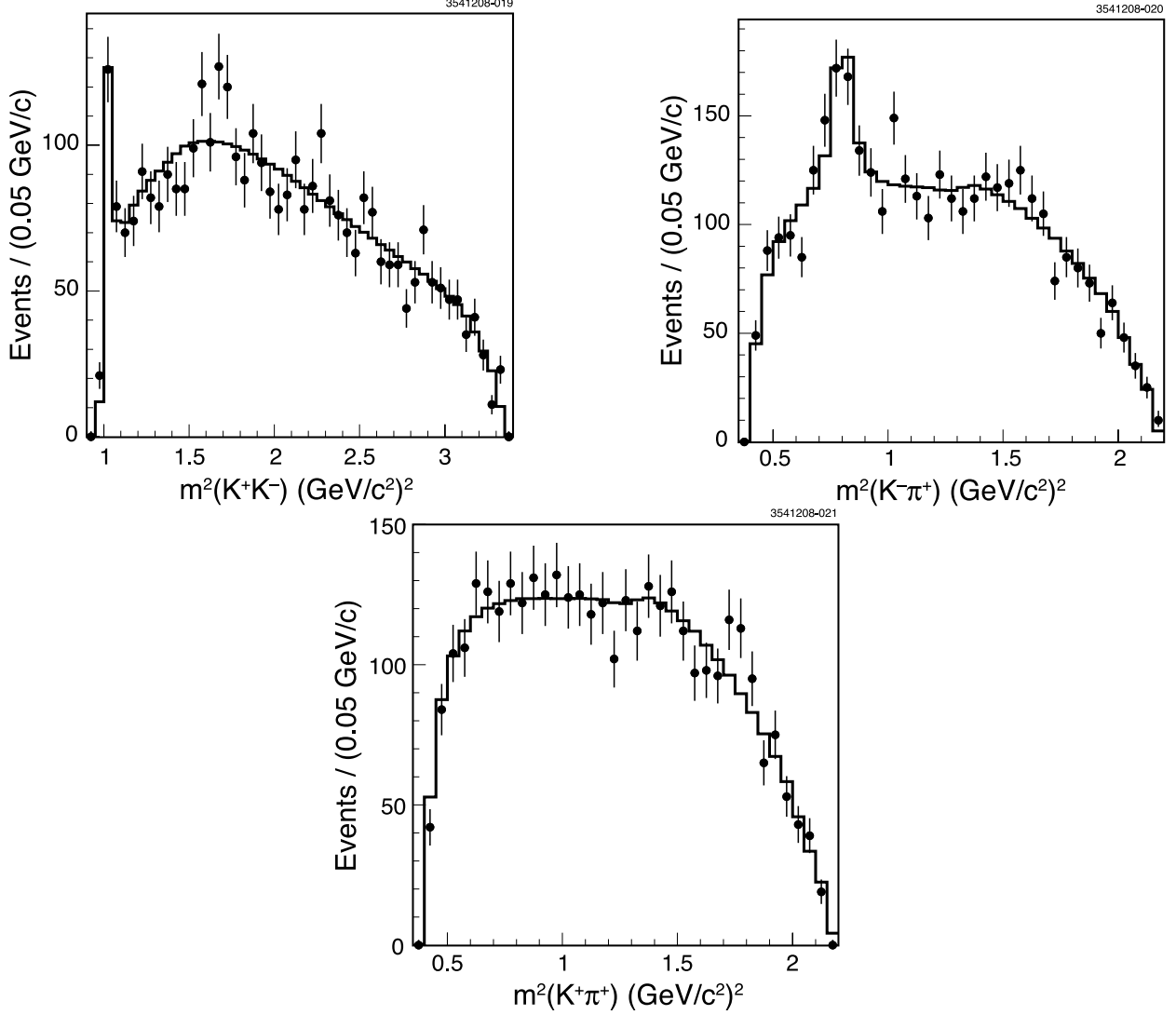


FIG. 3: Projections of the fit to the background shape described in the text, line, displayed over the data, dots, in the background box.

### III. FORMALISM

This Dalitz plot analysis employs the techniques and formalism described in Ref. [10] that have been applied in many other CLEO analyses. We use an unbinned maximum likelihood fit that minimizes the sum over  $N$  events:

$$\mathcal{L} = -2 \sum_{n=1}^N \log \mathcal{P}(x_n, y_n), \quad (6)$$

where  $\mathcal{P}(x, y)$  is the probability density function (p.d.f.), which depends on the event sample being fit,

$$\mathcal{P}(x, y) = \begin{cases} \mathcal{N}_\varepsilon \varepsilon(x, y) & \text{for efficiency;} \\ \mathcal{N}_B B(x, y) & \text{for background;} \\ f_{\text{sig}} \mathcal{N}_S |\mathcal{M}(x, y)|^2 \varepsilon(x, y) + (1 - f_{\text{sig}}) \mathcal{N}_B B(x, y) & \text{for signal.} \end{cases} \quad (7)$$

The shapes for the efficiency,  $\varepsilon(x, y)$ , and background,  $B(x, y)$ , are discussed in the previous section. The signal p.d.f. is proportional to the efficiency-corrected matrix element squared,  $|\mathcal{M}(x, y)|^2$ . As described above, the signal fraction,  $f_{\text{sig}}$ , is defined from the invariant mass spectrum. The background term has a relative  $(1 - f_{\text{sig}})$  fraction. The efficiency, signal, and background fractions are normalized separately,  $1/\mathcal{N}_\varepsilon = \int \varepsilon(x, y) dx dy$ ,  $1/\mathcal{N}_S = \int |\mathcal{M}(x, y)|^2 \varepsilon(x, y) dx dy$ ,  $1/\mathcal{N}_B = \int B(x, y) dx dy$ , which provides the overall p.d.f. normalization,  $\int \mathcal{P}(x, y) dx dy = 1$ . The matrix element is a sum of partial amplitudes,

$$\mathcal{M} = \sum_R c_R \times \mathcal{W}_R \times \Omega_R \times \mathcal{F}_D^L \times \mathcal{F}_R^L, \quad (8)$$

where  $\mathcal{W}_R$  depends on the spin of resonance  $R$ . The factor  $\Omega_R$  is the angular distribution for the resonance, and the factors  $\mathcal{F}_D^L$  and  $\mathcal{F}_R^L$  are the Blatt-Weisskopf angular momentum barrier-penetration factors [11]. In our standard fit the complex factor  $c_R = a_R e^{i\phi_R}$  is represented by two real numbers, an amplitude  $a_R$  and a phase  $\phi_R$ . These are included in the list of fit parameters and can be left to float freely or fixed.

Assuming the decay chain  $d \rightarrow Rc \rightarrow abc$  we may write the angular distribution,

$$\begin{aligned} \Omega_R^{L=0} &= 1, \\ \Omega_R^{L=1} &= m_{bc}^2 - m_{ac}^2 + \frac{(m_d^2 - m_c^2)(m_a^2 - m_b^2)}{m_{ab}^2}, \\ \Omega_R^{L=2} &= [\Omega_R^{L=1}]^2 - \frac{1}{3} \left( m_{ab}^2 - 2m_d^2 - 2m_c^2 + \frac{(m_d^2 - m_c^2)^2}{m_{ab}^2} \right) \left( m_{ab}^2 - 2m_a^2 - 2m_b^2 + \frac{(m_a^2 - m_b^2)^2}{m_{ab}^2} \right), \end{aligned} \quad (9)$$

where  $m_d$  is the mass of the decaying particle and  $m_a$ ,  $m_b$  and  $m_c$  are the masses of the daughters;  $m_{ab}$ ,  $m_{ac}$ , and  $m_{bc}$  are the relevant invariant masses. These expressions for angular distributions can be obtained from covariant-tensor formalism or from orbital momentum partial waves decomposition using Legendre polynomials  $P_L(\cos\theta)$ , where  $\theta$  is the angle between particles  $a$  and  $c$  in the resonance  $R$  rest frame.

For regular resonances such as  $K^*(892)$ ,  $\phi(1020)$ ,  $K^*(1410)$ ,  $K_2^*(1430)$ , etc., we use the standard Breit-Wigner function,

$$\mathcal{W}_R(m) = \frac{1}{m_R^2 - m^2 - im_R \Gamma(m)} \quad (10)$$

multiplied by the angular distribution,  $\Omega_L$ , and the Blatt-Weisskopf form factors  $\mathcal{F}_D^L(q)$  and  $\mathcal{F}_R^L(q)$  for the  $D$ -meson and resonance  $R$  decay vertexes, respectively. We assume that the mass dependent width has the usual form

$$\Gamma(m) = \Gamma_R \frac{m_R}{m} \left( \frac{P}{P_R} \right)^{2L+1} [\mathcal{F}_R^L(P \times r_R)]^2, \quad (11)$$

where  $P$  is the decay products' momentum value in the decaying particle rest frame and  $r_R$  is the effective resonance radius. The form factors  $\mathcal{F}_D^L(q)$  and  $\mathcal{F}_R^L(q)$  in Eqs. 8 and 11 are defined in the Blatt-Weisskopf form [11]

$$L = 0 : \quad \mathcal{F}_V^0(q) = 1, \quad (12)$$

$$L = 1 : \quad \mathcal{F}_V^1(q) = \mathcal{N}_V^1 \times [1 + q^2]^{-1/2}, \quad (13)$$

$$L = 2 : \quad \mathcal{F}_V^2(q) = \mathcal{N}_V^2 \times [9 + 3q^2 + q^4]^{-1/2}, \quad (14)$$

where the label  $V$  stands for  $D$  or  $R$  decay vertex,  $q = P \times r_V$ ,  $r_V$  is an effective meson radius, and  $\mathcal{N}_V^L$  is a normalization constant defined by the condition  $\mathcal{F}_V^L(P_R \times r_V) = 1$ , where  $P_R$  is the products' momentum value at  $m = m_R$ .

The  $\mathcal{W}_R$  parameterization of the  $f_0(980)$ , whose mass,  $m_{f_0}$ , is close to the  $K\bar{K}$  production threshold, uses the Flatté [12] formula

$$\mathcal{W}_R(m) = \frac{1}{m_R^2 - m^2 - i \sum_{ab} g_{Rab}^2 \rho_{ab}(m)} \quad (15)$$

where  $ab$  stands for  $\pi^0\pi^0$ ,  $\pi^+\pi^-$ ,  $K^+K^-$ , and  $K^0\bar{K}^0$ , and  $\rho_{ab}(m) = 2P_a/m$  is a phase space factor, calculated for the decay products momentum,  $P_a$ , in the resonance rest frame. We use the following isospin relations for the coupling constants  $g_{f_0\pi^+\pi^-} = \sqrt{2/3}g_{f_0\pi\pi}$ ,  $g_{f_0\pi^0\pi^0} = \sqrt{1/3}g_{f_0\pi\pi}$ , and  $g_{f_0K^0\bar{K}^0} = g_{f_0K^+K^-} = \sqrt{1/2}g_{f_0K\bar{K}}$ . Their values, shown in Table III, are taken from the BES experiment [13].

We model a low mass  $K^+\pi^-$  S wave, also known as  $\kappa$  or  $K(800)$ , using a complex pole amplitude proposed in Ref. [14],

$$\mathcal{W}_\kappa(m) = \frac{1}{m_\kappa^2 - m^2}, \quad (16)$$

where  $m_\kappa = (0.71 - i0.32)$  GeV is a pole position in the complex  $s = m^2(K^+\pi^-)$  plane estimated from the results of several experiments.

In this analysis we use or test all known  $K^-\pi^+$  and  $K^+K^-$  resonances recognized by the Particle Data Group (PDG) [8] which can be observed in the phase space of the  $D_s^+ \rightarrow K^-K^+\pi^+$  decay. These are listed in Table III. One could expect a contribution in the  $K^+K^-$  mass spectrum from the  $f_0(980)$  and  $a_0(980)$  scalar resonances. Their  $K^+K^-$  mass spectra have similar, but not well defined shapes. If both amplitudes are allowed to float simultaneously in the fit, they show a huge destructive interference, which is sensitive to their shape parameters. The  $f_0(980)$  contribution dominates [8] in the  $D_s^+ \rightarrow \pi^+\pi^+\pi^-$  decay, which has a large branching fraction,  $\mathcal{B}(D_s^+ \rightarrow \pi^+\pi^+\pi^-) = (1.22 \pm 0.23)\%$ . The relevant coupled channel of the  $a_0(980)$  has not been observed in the  $D_s^+ \rightarrow \eta\pi^0\pi^+$  decay. In this analysis we consider the  $f_0(980)$  contribution only.

#### IV. FITS TO DATA

First, we analyze our data with the model used by E687 [1]. Their isobar model contains five contributions,  $K^*(892)^0K^+$ ,  $\phi(1020)\pi^+$ ,  $K_0^*(1430)K^+$ ,  $f_0(980)\pi^+$ , and  $f_0(1710)\pi^+$ . In our analysis of  $D^+ \rightarrow K^-\pi^+\pi^+$  and  $D^+ \rightarrow K^-K^+\pi^+$  decays we find a  $K^*(892)$  width that is smaller than the world average value from the PDG [8]. Thus we let the mass and width of  $K^*(892)$  float in the fit. Results are shown in Table IV. In this table and all succeeding tables, the units of the amplitudes are arbitrary (a.u.). We find that the sign of the  $\phi(1020)$  contribution is opposite to the sign obtained by E687, but all other results are consistent within quoted uncertainties. We find that this fit to our data sample has a poor  $\chi^2/\nu$ , where  $\nu$  is the number of degrees of freedom, giving a very small fit probability. The  $\chi^2$  is calculated over adaptive bins, similar to our previous analysis [15]. This model does not represent our data well especially in the range of  $1.1 < m_{KK}^2 < 1.5$  GeV<sup>2</sup>/c<sup>4</sup>.

The E687 model contains five resonances. Two of them,  $K^*(892)$  and  $\phi(1020)$ , are clearly seen on the Dalitz plot. The other three,  $K_0^*(1430)$ ,  $f_0(980)$ , and  $f_0(1710)$ , are too wide to

TABLE III: Parameters of contributing resonances.

Resonance	$J^{PC}$	Mass (MeV/ $c^2$ )	Width (MeV/ $c^2$ )
$K\pi$ states			
$K^*(892)$	$1^-$	$896.00 \pm 0.25$	$50.3 \pm 0.6$
$K^*(1410)$	$1^-$	$1414 \pm 15$	$232 \pm 21$
$K_0^*(1430)$	$0^+$	$1414 \pm 6$	$290 \pm 21$
$K_2^*(1430)$	$2^+$	$1432.4 \pm 1.3$	$109 \pm 5$
$K^*(1680)$	$1^-$	$1717 \pm 27$	$322 \pm 110$
$\kappa$	$0^+$	$\Re m = 710$	$\Im m = -310$
$K^+K^-$ states			
$f_0(980)$	$0^{++}$	$965 \pm 10$	$g_{\pi\pi} = 406$ $g_{KK} = 800$
$a_0(980)$	$0^{++}$	$999 \pm 1$	$g_{\eta\pi} = 620$ $g_{KK} = 500$
$\phi(1020)$	$1^{--}$	$1019.460 \pm 0.019$	$4.26 \pm 0.05$
$f_2(1270)$	$2^{++}$	$1275.4 \pm 1.1$	$185.2^{+3.1}_{-2.5}$
$a_2(1320)$	$2^{++}$	$1318.3 \pm 0.6$	$107 \pm 5$
$f_0(1370)$	$0^{++}$	1200 to 1500	200 to 500
$a_0(1450)$	$0^{++}$	$1474 \pm 19$	$265 \pm 13$
$f_0(1500)$	$0^{++}$	$1507 \pm 5$	$109 \pm 7$
$f_2(1525)$	$2^{++}$	$1525 \pm 5$	$73^{+6}_{-5}$
$f_0(1710)$	$0^{++}$	$1718 \pm 6$	$137 \pm 8$
$\phi(1680)$	$1^{--}$	$1680 \pm 20$	$150 \pm 50$

be easily discerned. To check their significance we remove them one-by-one from the total amplitude and check the fit results. In all fits where we remove one resonance the fit quality is degraded, increasing  $\chi^2/\nu$  by more than 0.6, compared to our central fit. Thus, we assume that all five resonances from E687 model are significant.

In order to get better consistency between the model and data, we try to improve the E687 model by adding contributions from the other known resonances listed in Table III. The results of these fits are shown in Tables V and VI as a variation of the fit parameters with respect to the central case. In all cases the fit quality is improved and each additional resonance has a significant magnitude. We conclude that the five resonance model based on E687 results does not fully describe the data sample. The largest fit quality improvement is achieved in the case of additional S-wave contributions:  $f_0(1370)$ ; non-resonant ( $NR$ );  $a_0(1450)$ ; and  $\kappa$ . Adding the  $f_0(1370)$  contribution gives the largest improvement of the fit quality,  $\Delta\chi^2 = -100$  for two fewer degrees of freedom.

We consider a six-resonance model, called Model A, containing  $K^*(892)^0 K^+$ ,  $\phi(1020)\pi^+$ ,  $K_0^*(1430)K^+$ ,  $f_0(980)\pi^+$ ,  $f_0(1710)\pi^+$ , and  $f_0(1370)\pi^+$  contributions. Model A is simply the E687 isobar model with an additional  $f_0(1370)\pi^+$  contribution. Results with this model and fit projections are shown in Fig. 4. We repeat the previous procedure and include one-by-one additional resonance and check the significance of its parameters and consistency of the p.d.f. with our data sample. Results are shown in Tables VII and VIII. For Model A we

TABLE IV: Comparison of CLEO-c results with E687 using the E687 isobar model. Shown are the fitted magnitudes,  $a$  in arbitrary units, the phases ( $\phi$ ) in degrees, defined relative to the  $K^*(892)^0\pi^+$  amplitude, and the fit fractions (FF).

Mode	Parameter	E687	CLEO-c [PDG]
$\overline{K}^*(892)^0 K^+$	$a$	(fixed)	1 (fixed)
	$\phi$ ( $^\circ$ )	0 (fixed)	0 (fixed)
	$m$ (MeV/ $c^2$ )		$895.8 \pm 0.5$ [ $896.00 \pm 0.25$ ]
	$\Gamma$ (MeV/ $c^2$ )		$44.2 \pm 1.0$ [ $50.3 \pm 0.06$ ]
	FF (%)	$47.8 \pm 4.6 \pm 4.0$	$48.2 \pm 1.2$
$\overline{K}_0^*(1430) K^+$	$a$	N/A	$1.76 \pm 0.12$
	$\phi$ ( $^\circ$ )	$152 \pm 40 \pm 39$	$145 \pm 8$
	FF (%)	$9.3 \pm 3.2 \pm 3.2$	$5.3 \pm 0.7$
$\phi(1020)\pi^+$	$a$	N/A	$1.15 \pm 0.02$
	$\phi$ ( $^\circ$ )	$178 \pm 20 \pm 24$	$-15 \pm 4$
	FF (%)	$39.6 \pm 3.3 \pm 4.7$	$42.7 \pm 1.3$
$f_0(980)\pi^+$	$a$	N/A	$3.67 \pm 0.13$
	$\phi$ ( $^\circ$ )	$159 \pm 22 \pm 16$	$156 \pm 3$
	FF (%)	$11.0 \pm 3.5 \pm 2.6$	$16.8 \pm 1.1$
$f_0(1710)\pi^+$	$a$	N/A	$1.27 \pm 0.07$
	$\phi$ ( $^\circ$ )	$110 \pm 20 \pm 17$	$102 \pm 4$
	FF (%)	$3.4 \pm 2.3 \pm 3.5$	$4.4 \pm 0.4$
$\sum$ FF (%)		111.1	$117.3 \pm 2.2$
Number of events on DP			14400
Number of Signal events		$701 \pm 36$	$12226 \pm 22$
Goodness	$\chi^2/\nu$	50.2/33	278/119

do not find any additional resonances with significant magnitude, the fit quality does not significantly improve, and thus we take this model for our central result. For each additional resonance we estimate an upper limit on its fit fraction at 90% confidence level, as also shown in Tables VII and VIII. We conclude that the six-resonance Model A p.d.f. gives a good description of our data sample.

For Model A we test the resonance shape parameters by floating the mass and width, or two coupling constants in case of  $f_0(980)$ , for each resonance. Results of these fits are shown in Tables IX and X. We find that all parameters are consistent with their central fit values used in the fit with Model A.

To estimate systematic uncertainties of the fit parameters, we apply numerous variations to the fitting procedure and look at the change of the fit parameters from the central result. We consider sub-samples where the data is split into earlier and later datasets,  $D_s^+$  and  $D_s^-$  decays, and selected using tight and loose signal boxes. These are shown in Table XI. These results are obtained with fixed parameters for efficiency and background functions from Tables I and II. We also consider fits with floating efficiency or background parameters in Table XII. In these fits all polynomial coefficients for the efficiency or background including resonance background amplitudes float freely, but we fit simultaneously two samples of

TABLE V: Fits to CLEO-c data using the E687 model with additional  $K^-\pi^+$  resonances. For the contributions that do not change the entries in the table are changes from the E687 model.

Parameter	E687 Model	$NR$	$K^*(1410)$	$K_2^*(1430)$	$K^*(1680)$	$\kappa$
$m_{K^*(892)}$	$895.8 \pm 0.5$	0.0	-0.4	-0.1	-1.2	-0.9
$\Gamma_{K^*(892)}$	$44.2 \pm 1.0$	0.4	-1.3	0.3	-2.1	-0.3
$a_{K_0^*(1430)}$ (a.u.)	$1.76 \pm 0.12$	-1.16	-0.02	0.14	0.05	-0.58
$\phi_{K_0^*(1430)}$ ( $^\circ$ )	$145 \pm 8$	-4.2	4	7.3	-4	-7
$a_{f_0(980)}$ (a.u.)	$3.67 \pm 0.13$	1.64	0.28	-0.19	0.69	0.91
$\phi_{f_0(980)}$ ( $^\circ$ )	$156 \pm 3$	41	-2.2	4.3	-0.78	29
$a_{\phi(1020)}$ (a.u.)	$1.15 \pm 0.02$	-0.02	0.04	0.003	0.06	-0.01
$\phi_{\phi(1020)}$ ( $^\circ$ )	$-15 \pm 4$	32	-13	0.6	-10.4	26
$a_{f_0(1710)}$ (a.u.)	$1.27 \pm 0.07$	-0.83	0.06	-0.07	0.22	-0.87
$\phi_{f_0(1710)}$ ( $^\circ$ )	$102 \pm 4$	-27	-9.4	3.0	-6.7	-15
$a_{\text{add}}$ (a.u.)		$5.2 \pm 0.4$	$1.77 \pm 0.21$	$0.92 \pm 0.15$	$6.3 \pm 0.9$	$2.27 \pm 0.17$
$\phi_{\text{add}}$ ( $^\circ$ )		$193 \pm 4$	$93 \pm 6$	$-179 \pm 16$	$117 \pm 9$	$51 \pm 4$
$\chi^2/\nu$	278/119	192/117	249/117	241/117	256/117	200/117

TABLE VI: Fits to CLEO-c data using the E687 model with additional  $K^+K^-$  resonances. For the contributions that do not change the entries in the table are changes from the E687 model.

Parameter	E687 Model	$f_2(1270)$	$a_2(1320)$	$f_0(1370)$	$f_0(1500)$	$f_2(1525)$	$a_0(1450)$	$\phi(1680)$
$m_{K^*(892)}$	$895.8 \pm 0.5$	-0.4	-0.1	-0.9	-0.5	0.0	-0.8	0.1
$\Gamma_{K^*(892)}$	$44.2 \pm 1.0$	2.3	2.4	1.5	0.6	0.6	1.0	1.2
$a_{K_0^*(1430)}$ (a.u.)	$1.76 \pm 0.12$	0.11	0.08	-0.25	-0.03	-0.16	-0.22	-0.18
$\phi_{K_0^*(1430)}$ ( $^\circ$ )	$145 \pm 8$	-32	-28	1.0	-15	1.7	-15	18
$a_{f_0(980)}$ (a.u.)	$3.67 \pm 0.13$	0.29	0.26	1.05	0.52	0.03	1.09	0.20
$\phi_{f_0(980)}$ ( $^\circ$ )	$156 \pm 3$	-2	-1.6	1.3	2.3	0.22	3.8	10.5
$a_{\phi(1020)}$ (a.u.)	$1.15 \pm 0.02$	-0.03	-0.04	-0.02	-0.003	-0.02	-0.007	-0.012
$\phi_{\phi(1020)}$ ( $^\circ$ )	$-15 \pm 4$	-7	-6.3	7.2	-0.6	1.5	4.3	13.2
$a_{f_0(1710)}$ (a.u.)	$1.27 \pm 0.07$	0.08	0.07	-0.16	0.17	-0.04	0.03	-0.018
$\phi_{f_0(1710)}$ ( $^\circ$ )	$102 \pm 4$	7	4.7	-13	-4.1	-3.8	-17	5.3
$a_{\text{add}}$ (a.u.)		$0.64 \pm 0.09$	$0.45 \pm 0.06$	$1.15 \pm 0.09$	$0.50 \pm 0.05$	$0.50 \pm 0.07$	$1.32 \pm 0.10$	$1.04 \pm 0.17$
$\phi_{\text{add}}$ ( $^\circ$ )		$17 \pm 9$	$40 \pm 8$	$53 \pm 5$	$132 \pm 7$	$173 \pm 10$	$103 \pm 5$	$-4 \pm 11$
$\chi^2/\nu$	278/119	237/117	237/117	178/117	229/117	249/117	192/117	256/117

events for data plus the signal MC efficiency or background box to constrain the variation of the efficiency or background parameters. We also fit allowing the signal fraction to float, and find  $f_{\text{sig}} = 0.8495 \pm 0.0070$  which is consistent with 0.8490 used in the central fit.

We estimate a systematic uncertainty of the Model A fit parameters by combining the fit results from Tables VII, VIII, X, XI, and XII. None of the systematic variations dominate

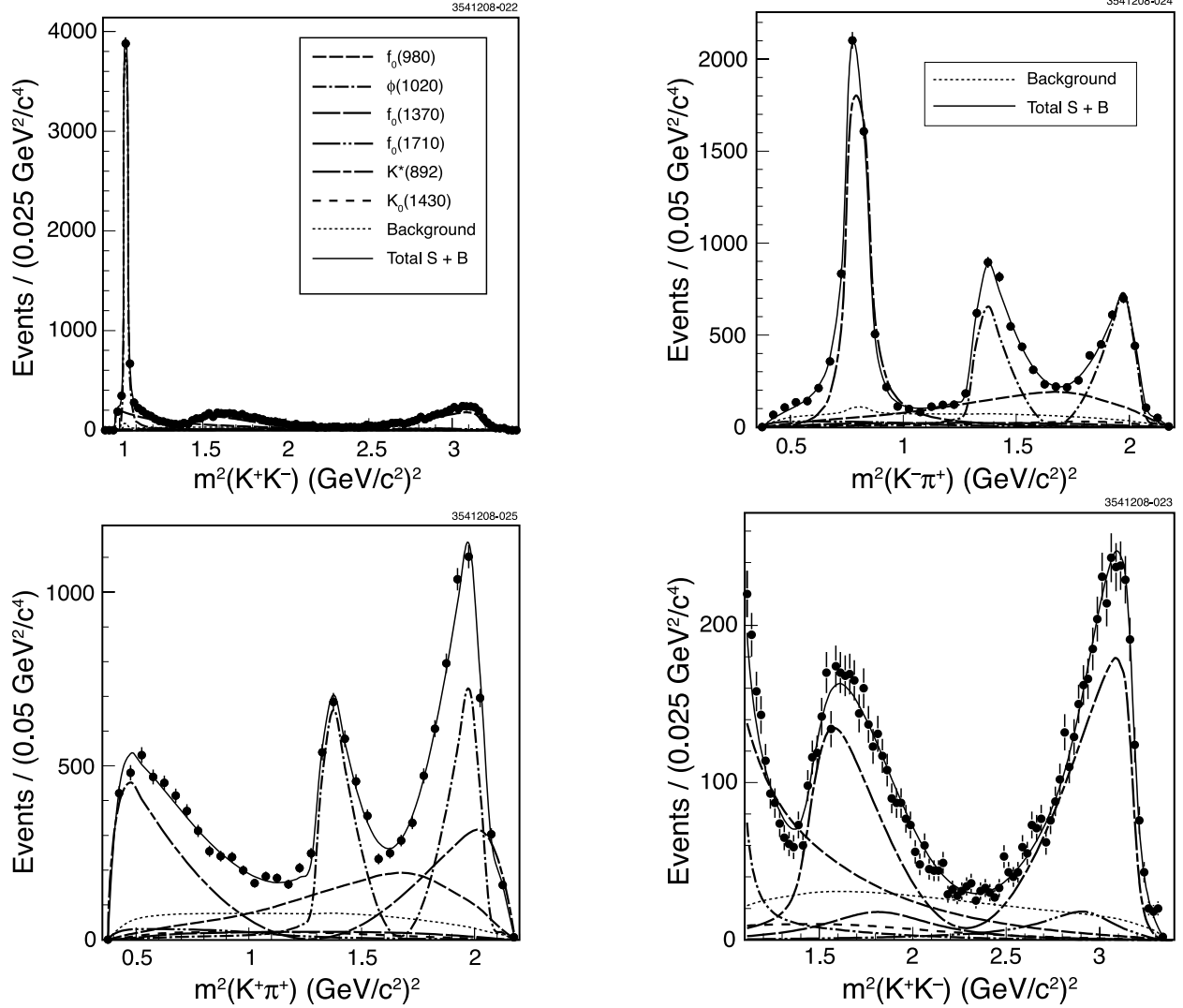


FIG. 4: Fit to data for Model A, and projections of the Dalitz plot. The final plot shows the  $m^2(KK)$  projection of Dalitz plot for values of  $m^2(KK)$  larger than the contribution from the  $\phi(1020)$ .

the uncertainty. The systematic uncertainty is estimated as the mean change from the central fit result,  $\delta Mean$ , added in quadrature to the RMS of all variations. The resulting systematic uncertainties on the parameters are given in Table XIII.

## V. CONCLUSION

We perform a Dalitz plot analysis of the  $D_s^+ \rightarrow K^+ K^- \pi^+$  decay with the CLEO-c data set of  $586 \text{ pb}^{-1}$  of  $e^+e^-$  collisions accumulated at  $\sqrt{s} = 4.17 \text{ GeV}$ . This corresponds to about 0.57 million  $D_s^+ D_s^{*-}$  pairs from which we select 14400 candidate events with a background of 15%. We compare our results with the previous measurement from E687 using the isobar model and find good agreement with the E687 parameters, as shown in Table IV. We find that all resonances from E687 model are significant and their exclusion degrades the fit

TABLE VII: Fits to data using Model A with additional non-resonant or  $K^+\pi^-$  resonance. For the contributions that do not change the entries in the table are changes from Model A.

Parameter	Model A	$NR$	$K^*(1410)$	$K_2^*(1430)$	$K^*(1680)$	$\kappa$
$m_{K^*(892)}$	$894.9 \pm 0.5$	0.3	0.1	0.2	0.2	-0.1
$\Gamma_{K^*(892)}$	$45.7 \pm 1.1$	-0.1	0.1	0.8	0.6	-0.3
$a_{K_0^*(1430)}$ (a.u.)	$1.51 \pm 0.11$	-0.1878	-0.0245	0.0603	-0.1434	0.2685
$\phi_{K_0^*(1430)}$ ( $^\circ$ )	$146 \pm 8$	-10.833	0.4446	-4.8755	2.3676	-7.6608
$a_{f_0(980)}$ (a.u.)	$4.72 \pm 0.18$	-0.0529	0.0057	0.2566	-0.2530	-0.2078
$\phi_{f_0(980)}$ ( $^\circ$ )	$157 \pm 3$	8.1153	-0.7457	1.0875	1.7545	-4.5506
$a_{\phi(1020)}$ (a.u.)	$1.13 \pm 0.02$	-0.0005	-0.0001	-0.0096	-0.0159	0.0047
$\phi_{\phi(1020)}$ ( $^\circ$ )	$-8 \pm 4$	3.9973	-0.1144	-4.8349	5.2172	-5.0235
$a_{f_0(1370)}$ (a.u.)	$1.15 \pm 0.09$	-0.0979	-0.0055	0.0535	0.0103	0.0890
$\phi_{f_0(1370)}$ ( $^\circ$ )	$53 \pm 5$	5.5500	-1.6829	-4.4427	3.2688	-11.386
$a_{f_0(1710)}$ (a.u.)	$1.11 \pm 0.07$	-0.1502	-0.0093	-0.0157	-0.0442	-0.0940
$\phi_{f_0(1710)}$ ( $^\circ$ )	$89 \pm 5$	-7.3126	-1.2087	3.7678	2.4526	-6.2195
$a_{\text{add}}$ (a.u.)	0	$1.3 \pm 0.6$	$0.10 \pm 0.13$	$1.00 \pm 0.26$	$2.18 \pm 1.33$	$0.50 \pm 0.18$
$\phi_{\text{add}}$ ( $^\circ$ )	0	$-147 \pm 19$	$-3 \pm 119$	$105 \pm 11$	$-72 \pm 13$	$163 \pm 25$
$\text{FF}_{\text{add}}$ (%)	0	$1.5 \pm 1.4$	$0.01 \pm 0.03$	$0.40 \pm 0.22$	$0.30 \pm 0.44$	$0.40 \pm 0.32$
$\text{FF}_{\text{add}}$ (%) @ 90% C.L.	0	<3.3%	<0.05%	<0.7%	<0.9%	<0.8%
$\text{FF}[K^*(892)]$ (%)	$47.4 \pm 1.5$	47.5	47.5	47.8	48.3	47.5
$\text{FF}[K_0^*(1430)]$ (%)	$3.9 \pm 0.5$	3.0	3.8	4.4	3.3	5.5
$\text{FF}[f_0(980)]$ (%)	$28.2 \pm 1.9$	27.7	28.4	32.3	26.2	25.7
$\text{FF}[\phi(1020)]$ (%)	$42.2 \pm 1.6$	41.9	42.1	42.3	42.1	42.1
$\text{FF}[f_0(1370)]$ (%)	$4.3 \pm 0.6$	3.5	4.2	4.8	4.5	4.9
$\text{FF}[f_0(1710)]$ (%)	$3.4 \pm 0.5$	2.6	3.4	3.4	3.3	2.9
$\sum_R \text{FF}_R$ (%)	129.5	127.8	129.4	135.4	127.9	129.0
$\chi^2/\nu$	178/117	174/115	177/115	170/115	175/115	173/115

quality.

However, the fit quality is significantly improved if we add an additional  $K^+K^-$  resonance to the model. As shown in Tables V and VI, almost any additional resonance or non-resonant contribution improves the agreement with the data. The best improvement is achieved if we add an  $f_0(1370)\pi^+$  contribution. We find that a six-resonance model, containing contributions from  $K^*(892)^0K^+$ ,  $K_0^*(1430)K^+$ ,  $f_0(980)\pi^+$ ,  $\phi(1020)\pi^+$ ,  $f_0(1370)\pi^+$ , and  $f_0(1710)\pi^+$  resonances, gives better consistency with our data with  $\chi^2/\nu = 178/117$ . Tables VII and VIII show that any further additional resonance does not have a significant amplitude, fit fraction, or significantly improve the fit quality and we give upper limits on their fit fractions at the 90% C.L.

In Table IX we show the resonance parameters when they are allowed to float in the fit. We find that the  $K^*(892)$  width is 5 MeV/ $c^2$  smaller than in PDG. This result is consistent with our observation in the  $D^+ \rightarrow K^-\pi^+\pi^+$  analysis [15]. Other resonance parameters are consistent with their values from the PDG [8] or the BES experiment [13] for  $f_0(980)$ .

We estimate a systematic uncertainty on fit parameters from numerous fit variations,



TABLE VIII: Fits using Model A with additional  $K^+K^-$  resonance. For the contributions that do not change the entries in the table are changes from Model A.

Parameter	Model A	$f_2(1270)$	$a_2(1320)$	$f_0(1500)$	$f_2(1525)$	$a_0(1450)$	$\phi(1680)$
$m_{K^*(892)}$	$894.9 \pm 0.5$	-0.5	-0.3	-0.1	-0.2	-0.1	-0.1
$\Gamma_{K^*(892)}$	$45.7 \pm 1.1$	1.2	1.2	-0.1	0.2	-0.1	-0.2
$a_{K_0^*(1430)}$ (a.u.)	$1.51 \pm 0.11$	-0.0518	-0.0587	-0.0060	-0.0822	-0.0210	-0.0152
$\phi_{K_0^*(1430)}$ ( $^\circ$ )	$146 \pm 8$	-13.610	-7.5258	1.1483	0.1662	2.4740	-0.8833
$a_{f_0(980)}$ (a.u.)	$4.72 \pm 0.18$	0.0864	-0.0037	0.0521	-0.0239	0.1123	0.0113
$\phi_{f_0(980)}$ ( $^\circ$ )	$157 \pm 3$	-0.6746	-0.6856	0.6617	-0.3009	1.1151	-0.1360
$a_{\phi(1020)}$ (a.u.)	$1.13 \pm 0.02$	-0.0105	-0.0126	0.0058	-0.0058	0.0068	0.0056
$\phi_{\phi(1020)}$ ( $^\circ$ )	$-8 \pm 4$	-2.1292	-1.5385	0.5046	-0.1244	1.2202	-0.4788
$a_{f_0(1370)}$ (a.u.)	$1.15 \pm 0.09$	-0.0176	-0.0343	0.0336	-0.0168	0.0150	-0.0039
$\phi_{f_0(1370)}$ ( $^\circ$ )	$53 \pm 5$	1.0892	-0.3964	3.8125	1.4021	14.6004	0.3390
$a_{f_0(1710)}$ (a.u.)	$1.11 \pm 0.07$	0.0041	-0.0165	-0.0161	-0.0100	-0.0533	0.0007
$\phi_{f_0(1710)}$ ( $^\circ$ )	$89 \pm 5$	4.7785	2.7846	-1.9584	-2.2626	-3.6665	-0.9276
$a_{\text{add}}$ (a.u.)	0	$0.40 \pm 0.09$	$0.26 \pm 0.06$	$0.07 \pm 0.04$	$0.23 \pm 0.08$	$0.37 \pm 0.28$	$0.10 \pm 0.16$
$\phi_{\text{add}}$ ( $^\circ$ )	0	$22 \pm 14$	$51 \pm 15$	$37 \pm 66$	$180 \pm 26$	$24 \pm 17$	$-93 \pm 122$
FF <sub>add</sub> (%)	0	$0.24 \pm 0.11$	$0.20 \pm 0.09$	$0.04 \pm 0.10$	$0.09 \pm 0.05$	$0.38 \pm 0.60$	$0.008 \pm 0.031$
FF <sub>add</sub> (%) @ 90% C.L.	0	<0.4%	<0.3%	<0.17%	<0.16%	<1.2%	<0.05%
FF[ $K^*(892)$ ] (%)	$47.4 \pm 1.5$	47.2	47.4	47.3	48.0	47.3	47.4
FF[ $K_0^*(1430)$ ] (%)	$3.9 \pm 0.5$	3.8	3.7	3.9	3.6	3.8	3.8
FF[ $f_0(980)$ ] (%)	$28.2 \pm 1.9$	30.0	29.0	28.8	28.4	29.4	28.2
FF[ $\phi(1020)$ ] (%)	$42.2 \pm 1.6$	42.1	42.2	42.2	42.1	42.2	42.1
FF[ $f_0(1370)$ ] (%)	$4.3 \pm 0.6$	4.2	4.1	4.5	4.2	4.3	4.2
FF[ $f_0(1710)$ ] (%)	$3.4 \pm 0.5$	3.5	3.4	3.3	3.4	3.1	3.4
$\sum_R \text{FF}_R$ (%)	129.5	131.1	130.2	130.0	129.8	130.5	129.3
$\chi^2/\nu$	178/117	169/115	170/115	177/115	172/115	176/115	178/115

and Table XIII shows the final results on fit parameters with their statistical and systematic uncertainties.

### Acknowledgments

We gratefully acknowledge the effort of the CESR staff in providing us with excellent luminosity and running conditions. D. Cronin-Hennessy and A. Ryd thank the A.P. Sloan Foundation. This work was supported by the National Science Foundation, the U.S. Department of Energy, the Natural Sciences and Engineering Research Council of Canada, and

TABLE IX: Optimal resonance parameters. The uncertainties for the CLEO-c results are statistical only.

Resonance Parameter (MeV/ $c^2$ )		Central Fit	Floated	PDG [8]
$K^*(892)$	$m$	$895.8 \pm 0.5$	$895.8 \pm 0.5$	$896.00 \pm 0.25$
	$\Gamma$	$44.2 \pm 1.0$	$44.2 \pm 1.0$	$50.3 \pm 0.6$
$K_0^*(1430)$	$m$	1414	$1422 \pm 23$	$1414 \pm 6$
	$\Gamma$	290	$239 \pm 48$	$290 \pm 21$
$f_0(980)$	$m$	965	$933 \pm 21$	$980 \pm 10$
	$g_{\pi\pi}$	406	$393 \pm 36$	$\Gamma=40$ to 100
	$g_{KK}$	800	$557 \pm 88$	
$\phi(1020)$	$m$	1019.460	$1019.64 \pm 0.05$	$1019.460 \pm 0.019$
	$\Gamma$	4.26	$4.780 \pm 0.14$	$4.26 \pm 0.05$
$f_0(1370)$	$m$	1350	$1315 \pm 34$	1200 to 1500
	$\Gamma$	265	$276 \pm 39$	200 to 500
$f_0(1710)$	$m$	1718	$1749 \pm 12$	$1718 \pm 6$
	$\Gamma$	137	$175 \pm 29$	$137 \pm 8$

the U.K. Science and Technology Facilities Council.

- 
- [1] P.L. Frabetti *et al.* (E687 Collaboration), Phys. Lett., B**351**, 591 (1995).
  - [2] J. Alexander *et al.* (CLEO Collaboration), Phys. Rev. Lett. **100**, 161804 (2008).
  - [3] R.H. Dalitz, Philos. Mag. **44**, 1068 (1953).
  - [4] A.M. Rahimi, Amplitude Analysis of the  $D^+, D_s^+ \rightarrow K^- K^+ \pi^+$  and  $D^0 \rightarrow K_S^0 K^+ K^-$  Final States, FERMILAB-THESIS-2000-13.
  - [5] S. Malvezzi, AIP Conf. Proc. 549, 569 (2002).
  - [6] G. Viehhauser, Nucl. Instrum. Methods A **462**, 146 (2001); D. Peterson *et al.*, Nucl. Instrum. Methods Phys. Res., Sect. A **478**, 142 (2002); Y. Kubota *et al.*, Nucl. Instrum. Methods Phys. Res., Sect. A **320**, 66 (1992); R.A. Briere *et al.* (CESR-c and CLEO-c Taskforces, CLEO-c Collaboration), Cornell University, LEPP Report No. CLNS 01/1742 (2001) (unpublished).
  - [7] S. Dobbs *et al.* (CLEO Collaboration), Phys. Rev. D**76**, 112001 (2007).
  - [8] W.-M. Yao *et al.*, Journal of Physics G **33**, 1 (2006).
  - [9] D.J. Lange, Nucl. Instrum. Methods Phys. Res., Sect. A **462**, 152 (2001).
  - [10] S. Kopp *et al.* (CLEO Collaboration), Phys. Rev. D**63**, 092001 (2001).
  - [11] J.M. Blatt and V.F. Weisskopf, *Theoretical Nuclear Physics*, Wiley, New York, 1951, p.361.
  - [12] S.M. Flatté, CERN/EP/PHYS 76-8, 15 April 1976; Phys. Lett. B.**63**, 224 (1976).
  - [13] M. Ablikim *et al.* (BES Collaboration), Phys. Lett. B.**607** 243 (2005).
  - [14] J.A. Oller, Phys. Rev. D **71**, 054030 (2005).
  - [15] G. Bonvicini *et al.* (CLEO Collaboration), Phys. Rev. D**78**, 052001 (2008).

TABLE X: Fits to data using Model A with floating resonance parameters. After the first column of data the entries in the table are changes from Model A when the parameters of resonance at the top of the column are allowed to float.

Parameter	Model A	$K^*(1430)$	$f_0(980)$	$\phi(1020)$	$f_0(1370)$	$f_0(1710)$
$m_{K^*(892)}$	$894.9 \pm 0.5$	-0.1	0	0.2	-0.1	0.1
$\Gamma_{K^*(892)}$	$45.7 \pm 1.1$	-0.1	0.2	0.1	0.0	-0.5
$a_{K_0^*(1430)}$ (a.u.)	$1.51 \pm 0.11$	-0.1449	-0.1527	0.0256	0.0533	-0.0305
$\phi_{K_0^*(1430)}$ ( $^\circ$ )	$146 \pm 8$	8.6060	-3.2558	10.2102	7.5225	-5.6685
$a_{f_0(980)}$ (a.u.)	$4.72 \pm 0.18$	-0.0576	-0.3873	-0.3073	-0.0540	0.1767
$\phi_{f_0(980)}$ ( $^\circ$ )	$157 \pm 3$	-1.1202	-13.584	0.0037	-1.2207	3.4058
$a_{\phi(1020)}$ (a.u.)	$1.13 \pm 0.02$	0.0058	-0.0018	0.0786	0.0037	0.0167
$\phi_{\phi(1020)}$ ( $^\circ$ )	$-8 \pm 4$	-0.8216	5.2291	1.5697	0.9613	1.3374
$a_{f_0(1370)}$ (a.u.)	$1.15 \pm 0.09$	0.0473	-0.0319	-0.0508	0.0293	-0.1248
$\phi_{f_0(1370)}$ ( $^\circ$ )	$53 \pm 5$	-2.5387	4.8538	-2.6304	-17.247	3.0673
$a_{f_0(1710)}$ (a.u.)	$1.11 \pm 0.07$	-0.0060	-0.0096	-0.0291	-0.0656	0.4223
$\phi_{f_0(1710)}$ ( $^\circ$ )	$89 \pm 5$	-1.9306	-1.2058	-2.4148	0.0913	20.0144
FF[ $K^*(892)$ ] (%)	$47.4 \pm 1.5$	47.3	47.2	47.4	47.5	46.8
FF[ $K_0^*(1430)$ ] (%)	$3.9 \pm 0.5$	3.8	3.2	4.1	4.2	3.7
FF[ $f_0(980)$ ] (%)	$28.2 \pm 1.9$	27.5	29.7	24.8	27.7	29.7
FF[ $\phi(1020)$ ] (%)	$42.2 \pm 1.6$	42.2	41.8	43.3	42.2	42.0
FF[ $f_0(1370)$ ] (%)	$4.3 \pm 0.6$	4.6	4.0	3.9	4.4	3.3
FF[ $f_0(1710)$ ] (%)	$3.4 \pm 0.5$	3.4	3.4	3.3	3.0	4.1
$\sum_R$ FF $_R$ (%)	129.5	128.8	129.2	126.8	129.0	129.5
$\chi^2/\nu$	178/117	177/115	169/114	168/115	176/115	166/115

TABLE XI: Fits to a variety of data samples using Model A with central efficiency and background. After the first column of data the entries in the table are changes from Model A with the variation indicated at the top of the column.

Variation Parameter	Central Fit Model A	Early Data	Late Data	Only $D_s^+$	Only $D_s^-$	Tight $1\sigma \times 1\sigma$	Loose $3\sigma \times 3\sigma$	Low Side Band	High Side Band
$m_{K^*(892)}$	894.9 $\pm$ 0.5	-0.4	3.0	-0.7	0.7	-0.2	0.2	-1.2	-1.4
$\Gamma_{K^*(892)}$	45.7 $\pm$ 1.1	0.1	0.0	-0.8	0.8	-0.2	1.0	4.8	2.2
$a_{K_0^*(1430)}$ (a.u.)	1.51 $\pm$ 0.11	0.0138	0.0177	-0.0023	0.0398	-0.0205	-0.1276	-0.8084	0.7309
$\phi_{K_0^*(1430)}$ ( $^\circ$ )	146 $\pm$ 8	-10.971	9.7985	-17.161	17.257	-6.2148	14.408	18.400	-66.057
$a_{f_0(980)}$ (a.u.)	4.72 $\pm$ 0.18	0.3277	-0.3513	0.0484	-0.0416	-0.0364	0.0244	0.6752	0.3610
$\phi_{f_0(980)}$ ( $^\circ$ )	157 $\pm$ 3	-1.3604	1.1808	-6.3697	6.6295	-4.5506	2.8515	3.1875	-23.699
$a_{\phi(1020)}$ (a.u.)	1.13 $\pm$ 0.02	0.0053	0.0008	0.0084	0.0011	0.0153	-0.0049	0.0079	0.0210
$\phi_{\phi(1020)}$ ( $^\circ$ )	-8 $\pm$ 4	-2.9134	2.2119	-8.3156	8.5410	-7.0696	5.5073	8.5766	-35.140
$a_{f_0(1370)}$ (a.u.)	1.15 $\pm$ 0.09	0.0976	-0.1031	-0.0131	0.0250	-0.1193	0.1395	0.5111	0.3938
$\phi_{f_0(1370)}$ ( $^\circ$ )	53 $\pm$ 5	-2.8318	2.2204	-4.6088	2.4167	-6.5716	-1.3470	-14.394	-28.267
$a_{f_0(1710)}$ (a.u.)	1.11 $\pm$ 0.07	0.0786	-0.0830	-0.0412	0.0483	0.0403	0.0070	0.1877	-0.3847
$\phi_{f_0(1710)}$ ( $^\circ$ )	89 $\pm$ 5	-3.3881	2.2247	0.1313	-0.5966	0.7797	2.6467	16.146	-5.0150
FF[ $K^*(892)$ ] (%)	47.4 $\pm$ 1.5	47.2	47.7	47.9	46.7	47.2	46.8	43.4	48.0
FF[ $K_0^*(1430)$ ] (%)	3.9 $\pm$ 0.5	4.0	4.1	3.9	4.2	3.8	3.3	0.9	8.3
FF[ $f_0(980)$ ] (%)	28.2 $\pm$ 1.9	32.1	24.4	28.6	27.9	27.6	28.8	37.6	31.5
FF[ $\phi(1020)$ ] (%)	42.2 $\pm$ 1.6	42.0	42.3	42.1	42.2	42.7	42.0	43.3	41.8
FF[ $f_0(1370)$ ] (%)	4.3 $\pm$ 0.6	5.0	3.5	4.1	4.5	3.4	5.4	9.0	7.4
FF[ $f_0(1710)$ ] (%)	3.4 $\pm$ 0.5	3.9	3.0	3.2	3.8	3.7	3.5	4.8	1.4
$\sum_R$ FF $_R$ (%)	129.5	134.2	124.9	129.7	129.2	128.3	129.9	138.9	138.4
$\chi^2/\nu$	178/117	134/117	203/117	166/117	123/117	155/117	201/117	140/117	138/117
Events on DP	14400	7334	7066	7233	7167	7200	19177	6682	7232
$f_{\text{sig}}$	0.8490	0.8518	0.8466	0.8496	0.8497	0.9238	0.7484	0.4338	0.5696

TABLE XII: Fits to data using Model A with floating efficiency and background coefficients, fits with floating  $f_{\text{sig}}$ , and with floating background coefficients  $B_{K^*}$  and  $B_\phi$  for the narrow resonance contributions to the background. After the first column of data the entries in the table are changes from Model A with the variation indicated at the top of the column.

Parameter	Model A	Float $E_i$	Float $B_i$	Float $f_{\text{sig}}$
$m_{K^*(892)}$	$894.9 \pm 0.5$	0	0.1	0
$\Gamma_{K^*(892)}$	$45.7 \pm 1.1$	0	-0.2	0
$a_{K_0^*(1430)}$ (a.u.)	$1.51 \pm 0.11$	-0.0018	-0.0121	0.0023
$\phi_{K_0^*(1430)}$ ( $^\circ$ )	$146 \pm 8$	0.1630	-1.6971	0.2116
$a_{f_0(980)}$ (a.u.)	$4.72 \pm 0.18$	-0.0026	-0.0332	-0.0043
$\phi_{f_0(980)}$ ( $^\circ$ )	$157 \pm 3$	0.3362	-0.6851	0.2704
$a_{\phi(1020)}$ (a.u.)	$1.13 \pm 0.02$	0.0034	-0.0007	0.0028
$\phi_{\phi(1020)}$ ( $^\circ$ )	$-8 \pm 4$	0.1282	-0.9907	-0.0391
$a_{f_0(1370)}$ (a.u.)	$1.15 \pm 0.09$	-0.0015	0.0112	0.0006
$\phi_{f_0(1370)}$ ( $^\circ$ )	$53 \pm 5$	0.1323	-0.5403	0.0792
$a_{f_0(1710)}$ (a.u.)	$1.11 \pm 0.07$	-0.0007	-0.0539	-0.0038
$\phi_{f_0(1710)}$ ( $^\circ$ )	$89 \pm 5$	-0.2072	-1.1088	-0.3882
FF[ $K^*(892)$ ] (%)	$47.4 \pm 1.5$	47.4	47.7	47.4
FF[ $K_0^*(1430)$ ] (%)	$3.9 \pm 0.5$	3.9	3.9	3.9
FF[ $f_0(980)$ ] (%)	$28.2 \pm 1.9$	28.2	28.1	28.2
FF[ $\phi(1020)$ ] (%)	$42.2 \pm 1.6$	42.2	42.2	42.2
FF[ $f_0(1370)$ ] (%)	$4.3 \pm 0.6$	4.2	4.4	4.3
FF[ $f_0(1710)$ ] (%)	$3.4 \pm 0.5$	3.4	3.1	3.4
$\sum_R \text{FF}_R$ (%)	129.5	129.4	129.3	129.4
$\chi^2/\nu$	178/117	679/562	270/188	178/116

TABLE XIII: Summary of systematic cross checks for Model A. Fit parameters are shown with their statistical and systematic uncertainty respectively. The “ $\delta$ Mean” and “RMS” account for variation of the fit parameters in the systematic cross checks as discussed in the text. The “Total” is a quadratic sum of “ $\delta$ Mean” and “RMS” and after rounding is the systematic uncertainty given in the second column. The results of the E687 Model are also shown for comparison.

Parameter	Model A	$\delta$ Mean	RMS	Total	E687 Model
$m_{K^*(892)}$	$894.9 \pm 0.5 \pm 0.7$	0.088	0.654	0.660	$895.8 \pm 0.5$
$\Gamma_{K^*(892)}$	$45.7 \pm 1.1 \pm 0.5$	0.148	0.499	0.520	$44.2 \pm 1.0$
$a_{K_0^*(1430)}$ (a.u.)	$1.51 \pm 0.11 \pm 0.09$	-0.024	0.089	0.092	$1.76 \pm 0.12$
$\phi_{K_0^*(1430)}$ ( $^\circ$ )	$146 \pm 8 \pm 8$	-0.623	8.442	8.465	$145 \pm 8$
$a_{f_0(980)}$ (a.u.)	$4.72 \pm 0.18 \pm 0.17$	-0.029	0.167	0.170	$3.67 \pm 0.13$
$\phi_{f_0(980)}$ ( $^\circ$ )	$157 \pm 3 \pm 4$	-0.343	4.036	4.051	$156 \pm 3$
$a_{\phi(1020)}$ (a.u.)	$1.13 \pm 0.02 \pm 0.02$	0.004	0.017	0.018	$1.15 \pm 0.02$
$\phi_{\phi(1020)}$ ( $^\circ$ )	$-8 \pm 4 \pm 4$	0.081	3.850	3.851	$-15 \pm 4$
$a_{f_0(1370)}$ (a.u.)	$1.15 \pm 0.09 \pm 0.06$	-0.003	0.063	0.063	
$\phi_{f_0(1370)}$ ( $^\circ$ )	$53 \pm 5 \pm 6$	-0.536	5.820	5.845	
$a_{f_0(1710)}$ (a.u.)	$1.11 \pm 0.07 \pm 0.10$	-0.004	0.098	0.098	$1.27 \pm 0.07$
$\phi_{f_0(1710)}$ ( $^\circ$ )	$89 \pm 5 \pm 5$	0.195	4.916	4.920	$102 \pm 4$
FF[ $K^*(892)$ ] (%)	$47.4 \pm 1.5 \pm 0.4$	0.016	0.357	0.4	$48.2 \pm 1.2$
FF[ $K_0^*(1430)$ ] (%)	$3.9 \pm 0.5 \pm 0.5$	0.036	0.460	0.5	$5.3 \pm 0.7$
FF[ $f_0(980)$ ] (%)	$28.2 \pm 1.9 \pm 1.8$	0.096	1.792	1.8	$16.8 \pm 1.1$
FF[ $\phi(1020)$ ] (%)	$42.2 \pm 1.6 \pm 0.3$	0.018	0.277	0.3	$42.7 \pm 1.3$
FF[ $f_0(1370)$ ] (%)	$4.3 \pm 0.6 \pm 0.5$	0.044	0.488	0.5	
FF[ $f_0(1710)$ ] (%)	$3.4 \pm 0.5 \pm 0.3$	0.044	0.311	0.3	$4.4 \pm 0.4$
$\sum_R \text{FF}_R$ (%)	$129.5 \pm 4.4 \pm 2.0$	0.020	1.981	2.0	$117.3 \pm 2.2$
$\chi^2/\nu$	178/117				278/119